J Therm Anal Calorim (2017) 130:1913–1924
DOI 10.1007/s10973-017-6498-7

Synthesis, formation mechanism and hydraulic activity of novel composite cements belonging to the system $CaO–Al_2O_3–ZrO_2$

Dominika Madej[1]

Received: 19 December 2016 / Accepted: 22 May 2017 / Published online: 6 June 2017

Abstract This paper describes a new approach for synthesizing novel composite cements belonging to the system $CaO–Al_2O_3–ZrO_2$ via the high-temperature reactions within the $Ca_7ZrAl_6O_{18}–Al_2O_3$ system and characterizes products using X-ray diffraction (XRD), Rietveld XRD quantification, infrared spectroscopy, scanning electron microscopy combined with energy-dispersive spectrometry and heat flow calorimetry techniques. Quantitative comparison of the phase transformation in the samples 25 mass% Al_2O_3–75 mass% $Ca_7ZrAl_6O_{18}$, 50 mass% Al_2O_3–50 mass% $Ca_7ZrAl_6O_{18}$ and 75 mass% Al_2O_3–25 mass% $Ca_7ZrAl_6O_{18}$ sintered in the temperature range 1300–1500 °C was presented. Detailed investigations of the reaction mechanism in the synthesis process in these samples show that calcium zirconium aluminate is unstable when it is heated with alumina, and it undergoes chemical reactions forming calcium aluminates with different CaO/Al_2O_3 molar ratios and Zr-bearing compounds ($CaZrO_3$ or ZrO_2). Probability of liquid-phase sintering of ceramics prepared from alumina and $Ca_7ZrAl_6O_{18}$ that provides particle rearrangement increases with increasing the CaO/Al_2O_3 mass ratio of composites. Specifically, this paper discusses composition design and microstructural characterization for achieving modern calcia–alumina–zriconia composite cements. A model that explains the chemical and microstructural changes within the $Ca_7ZrAl_6O_{18}–Al_2O_3$ system due to high temperature was proposed. This study extensively investigates the effects of the cement phase composition on the hydraulic activity in the Ca-aluminates and Zr-bearing compounds containing blended binder pastes.

✉ Dominika Madej
dmadej@agh.edu.pl

[1] Department of Ceramics and Refractories, Faculty of Materials Science and Ceramics, AGH University of Science and Technology, al. A. Mickiewicza 30, 30-059 Kraków, Poland

Graphical Abstract

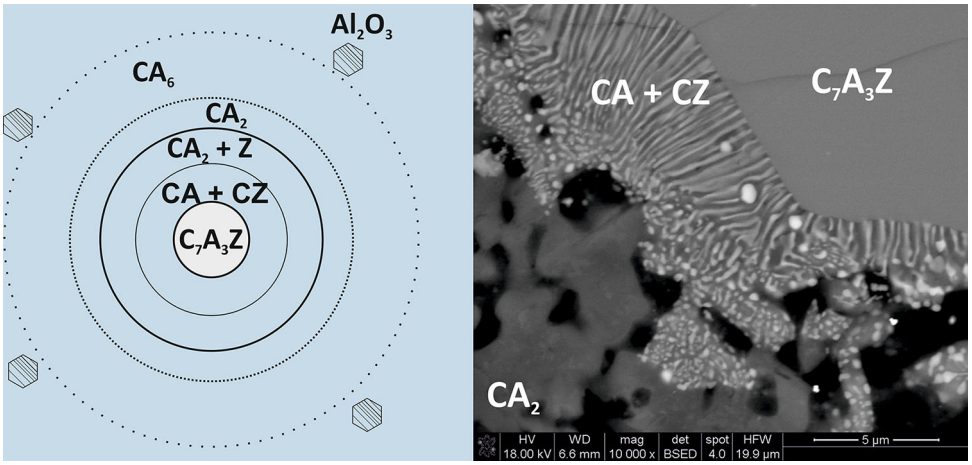

Keywords Calcium zirconium aluminate ($Ca_7ZrAl_6O_{18}$) · Calcium aluminates · Cement composition design · Hydration · Heat flow calorimetry

Introduction

Calcium monoaluminate ($CaAl_2O_4$, CA), calcium dialuminate ($CaAl_4O_7$, CA_2) and calcium hexa-aluminate ($CaAl_{12}O_{19}$, CA_6) are lime-alumina compounds involved in up-to-date ceramic technology and have attracted considerable attention due to their unique properties. CA (1606 °C) [1, 2] is the main chemically active hydraulic constituent of calcium aluminate cements (CACs) [3]. CA_2 is a compound which can be broadly used in modern refractories with a high resistance to thermal shock, especially due to its a high melting temperature (1759 °C) [1, 2] and very low or even negative coefficients of thermal expansion [4–6]. CA_6 is a non-hydraulic compound and more refractory than the other phases, having a melting point of 1850 °C [1, 2]. Calcium zirconium aluminate ($Ca_7ZrAl_6O_{18}$) having incongruent melting point at 1550 °C [7] has recently been analyzed in terms of its hydraulic properties [8–11]. Considering the above mentioned, the $CaO–Al_2O_3–ZrO_2$ multiphase composite cements can be recognized as very promising candidates for high-temperature applications.

There are several methods used for production of calcia–alumina–zirconia ceramics. Lee et al. [12] synthesized Al_2O_3-modified calcia-stabilized zirconia materials from fine powders by sintering at 1450–1600 °C in air atmosphere of green pellets shaped via uniaxial pressing and then isostatically pressed at 200 MPa. Liu et al. [13] prepared porous alumina–zirconia ceramics by infiltrating porous alumina ceramics previously prepared with ultrafine alumina powder via tert-butyl alcohol (TBA)-based gel-casting method. Ai et al. [14] fabricated zirconia matrix ceramics doped with 7.5 vol% nano-Al_2O_3 by two-step microwave sintering, two-step conventional sintering and one-step microwave sintering. According to a research paper discussing the formation mechanism of calcium aluminate compounds ($Ca_3Al_2O_6$, $Ca_5Al_6O_{14}$, $Ca_{12}Al_{14}O_{33}$, $CaAl_2O_4$, $CaAl_4O_7$ and $CaAl_{12}O_{19}$) based on high-temperature solid-state reaction within the temperature ranges 1100–1400 °C, CaO gradually diffuses into the Al_2O_3 core and then a layered distribution of calcium aluminates occurs [15]. Composites of $ZrO_2–CaAl_4O_7$ (CA_2) were synthesized by Bruni et al. [16] using the conventional sintering technique at 1400 °C from the mixture of monoclinic polymorph of zirconia with different amount of calcium aluminate cement (CAC). Calcium hexaluminate ($CaAl_{12}O_{19}$, CA_6, hibonite) in an elongated grain morphology was formed in situ during sintering of zirconia-toughened alumina ceramics with CaO at 1600 °C for 4 h [17]. The $CA_6–CA_2–Al_2O_3$ three-phase composite was also recently synthesized by the solid-state reaction process at an elevated temperature using the previously synthesized CA_2 compound and commercial corundum powder as starting materials [18]. They are also known the low thermal expansion ceramics based on calcium dialuminate ($CaAl_4O_7$, CA_2), calcium dialuminate-calcium zirconate ($CaZrO_3$, CZ) and calcium dialuminate–magnesium aluminate ($MgAl_2O_4$, MA) binary phases materials from the literature [4–6].

Thus, the present work was aimed at studying of the high-temperature reactions between $Ca_7ZrAl_6O_{18}$ and Al_2O_3 for obtaining of novel composite cements belonging to the system $CaO–Al_2O_3–ZrO_2$ with favorable hydraulic properties by in situ synthesis method. This approach to the composition and microstructural designs strategies is also a somewhat novel concept for the materials scientist.

Experimental

Materials and cements preparation procedure

The materials used in this study were a commercially available α-Al_2O_3 (PFR 20 reactive alumina, supplied by Alteo) with the chemical and physical characteristic given in Table 1 and calcium zirconium aluminate, $Ca_7ZrAl_6O_{18}$ (C_7A_3Z; $C \equiv CaO$, $A \equiv Al_2O_3$, $Z \equiv ZrO_2$). High-purity commercial mono-modal reactive alumina powder was used as a raw material for the preparation of binary mixtures of Al_2O_3 and $Ca_7ZrAl_6O_{18}$. For this work, $Ca_7ZrAl_6O_{18}$ was obtained by a two-step synthesis procedure. In a first step, the calcium carbonate (99.81% $CaCO_3$, Chempur), α-Al_2O_3 (99.8% Al_2O_3, Across Organics) and zirconia (98.08% ZrO_2, Merck) powders were mixed with the 7:3:1 molar ratio of CaO, Al_2O_3 and ZrO_2 oxides, and then, the mixture was homogenized for 2 h in a ball mil and pressed into cylinders having a diameter of 2 cm. All green pellets were calcined at 1200 °C for 10 h. In a second step, solid-state sintering of the pellets made from the calcined powder at 1500 °C for 30 h resulted in a single-phase orthorhombic $Ca_7ZrAl_6O_{18}$ structure. An intermediate grinding/mixing stage in order to improve homogeneity was necessary. Nevertheless, some trace impurities, in the form of $CaZrO_3$ and $Ca_{12}Al_{14}O_{33}$ were detected.

As a next step, novel calcia–zirconia–alumina pellets were prepared by a high-temperature reactive sintering of before synthesized $Ca_7ZrAl_6O_{18}$ and reactive Al_2O_3 micropowder. The initial compositions of the $Ca_7ZrAl_6O_{18}$–Al_2O_3 mixtures were located within the $Ca_7ZrAl_6O_{18}$–$CaAl_2O_4$–$CaZrO_3$, $CaAl_2O_4$–$CaAl_4O_7$–$CaZrO_3$ and $CaAl_4O_7$–$CaAl_{12}O_{19}$–ZrO_2 composition triangles of a ternary system CaO–Al_2O_3–ZrO_2. They contained 25, 50 or 75% by mass of Al_2O_3 and 75, 50 or 25% by mass of $Ca_7ZrAl_6O_{18}$, respectively. Homogenization of the mixtures proceeded for 2 h. Densification of the mixed powders was conducted by pressureless sintering of pellet samples at temperatures of 1300–1500 °C under air atmosphere (Table 2). The aluminates $CaAl_2O_4$ (CA), $CaAl_4O_7$ (CA_2) and $Ca_{12}Al_{14}O_{33}$ ($C_{12}A_7$) were also synthesized by two-cycle heating and grinding stoichiometric mixtures of $CaCO_3$ and Al_2O_3 for use as reference material for calorimetric studies.

Table 1 Chemical and physical characteristics of reactive alumina micropowder [19]

Chemical characteristic/mass%			Physical characteristic		
Na_2O total	SiO_2	Fe_2O_3	d_{50}/μm	d_{90}/μm	BET/m^2g^{-1}
0.05	0.1	0.015	2	4	1.9

Methods

X-ray diffraction analysis (XRD) was carried out using the X'Pert Pro PANalytical X-ray diffractometer. The XRD patterns of previously synthesized calcium zirconium aluminate phase, reactive alumina, calcium aluminates and calcia–zirconia–alumina composite cements were collected by step scanning with step of 0.02° over the range 2Θ 5°–90° at room temperature.

The phases developed during sintering were compared and confirmed using search–match reference ICDD database. Multiphase Rietveld phase quantification was also done using standard ICSD files supported by the PANalytical HighScore Plus software [20]. Goodness of fit (GOF) values lower than 2 proved a good quality Rietveld refinement for all samples. Various functional groups present in the prepared composite cements were identified by FT-IR. A Bruker Vertex 70v spectrometer was employed for this purpose. The FT-IR spectrometer was operated in the mid-IR region (4000–400 cm^{-1}) with a resolution of 4 cm^{-1}. Each spectrum represents the average of 128 scans. Samples were prepared by the standard KBr pellet method. Moreover, scanning electron microscopy (SEM, Nova NanoSEM 200 FEI) combined with energy-dispersive X-ray spectroscopy (EDS) was used to examine the microstructure development. For this purpose, resin-embedded samples were polished, coated with carbon to be conductive and then examined by SEM.

For microcalorimetric measurements, the pellets were ground and milled to obtain fine powder. Specific surface and grain size distribution of samples were measured by a laser diffraction analyzer (the Master Sizer 2000 Ver. 5.60 apparatus of Malvern (UK)). Heat of hydration of the novel composite cements belonging to the system CaO–Al_2O_3–ZrO_2 (Tables in Fig. 1a–c) and the reference aluminate phases was determined with a TAM Air microcalorimeter (TA Instruments) by integrating the continuous heat flow signal during the 20-h hydration process. Calorimetric measurements of synthetic cements were performed using

Table 2 Percentage composition (% by mass) of ceramic pellet samples and sintering condition

Sample	Component/mass%	
	Al_2O_3	$Ca_7ZrAl_6O_{18}$
25A–75C_7A_3Z	25	75
50A–50C_7A_3Z	50	50
75A–25C_7A_3Z	75	25

Sintering condition: 1300 °C (1 h), 1400 °C (1 h) and 1500 °C (1 and 3 h)

the in situ mixing treatments of the binder pastes under the following conditions: temperature of 25 °C and a water/-solid mass ratio w/s = 1.0. Tests were performed by mixing the pastes inside the calorimeter to allow the study of cement early hydration processes. For this purpose, two grams of dry powder was poured into a glass vial, and water weighed into mounted syringes. Admix ampoule was introduced into the calorimeter prior mixing, thus equilibrating to isothermal environment. Mixing was done after equilibration inside the calorimeter to enable the quantitative access to the heat of the early hydration process. A second glass vial containing sand (providing the same heat capacity that the mass of binder paste) was used as an inert reference in the twin channel of calorimeter to ensure the best stability of the baseline. Heat flow curves were normalized to the mass of total dry binder and reported in terms of power (mW g^{-1} dry binder) versus time (hours).

Results and discussion

Phase transformation

Phase transformation of samples 25A–75C_7A_3Z, 50A–50C_7A_3Z and 75A–25C_7A_3Z sintered in the temperature range 1300–1500 °C was examined by XRD analysis, and the crystalline phase content in the samples as determined by Rietveld refinements of the powder patterns is summarized in the tables presented in Fig. 1a–c.

Analysis of the quantitative phase changes based on the Rietveld XRD quantification shown in Fig. 1a–c is suitable to draw some reliable conclusions related to the mechanism of the reaction within the $Ca_7ZrAl_6O_{18}$–Al_2O_3 system in question. Now let us consider 25A–75C_7A_3Z sample (Fig. 1a). Calcium zirconium aluminate ($Ca_7ZrAl_6O_{18}$) reacted with Al_2O_3 to form calcium monoaluminate ($CaAl_2O_4$) and calcium zirconate ($CaZrO_3$)

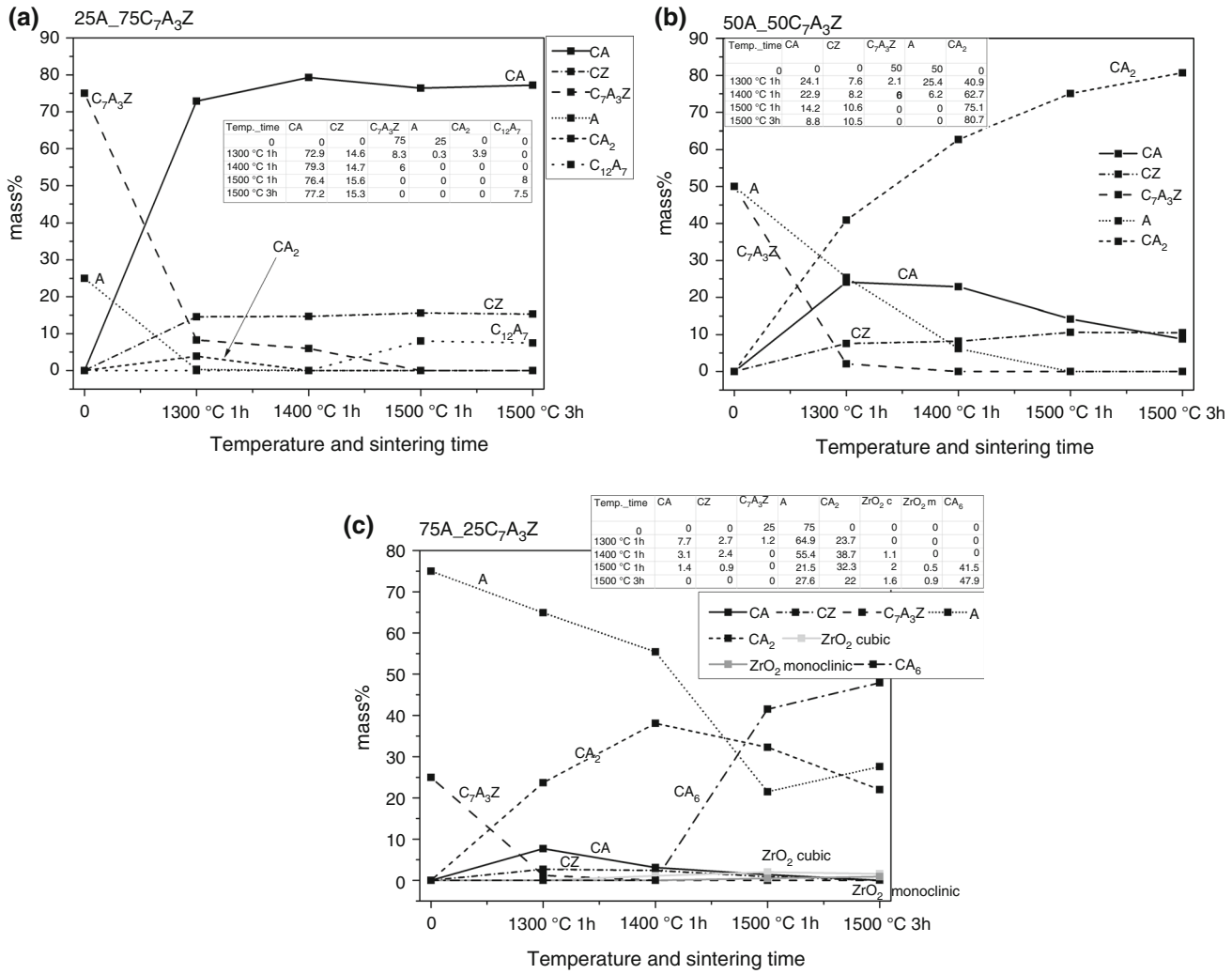

Fig. 1 The results of quantitative Rietveld analyses made with HighScore Plus (PANalytical) program for the samples 25A–75C_7A_3Z (**A**), 50A–50C_7A_3Z (**B**) and 75A–25C_7A_3Z (**C**) sintered in the temperature range 1300–1500 °C; C ≡ CaO, A ≡ Al_2O_3 and Z ≡ ZrO_2

following sintering at 1300 °C for 1 h. The same applies for the samples 50A–50C_7A_3Z and 75A–25C_7A_3Z where the content of $CaAl_2O_4$ also increases and the contents $Ca_7ZrAl_6O_{18}$ and Al_2O_3 accordingly decrease (Fig. 1b–c). The reaction proceeds according to Eq. 1.

$$Ca_7ZrAl_6O_{18} + 3Al_2O_3 \rightarrow 6CaAl_2O_4 + CaZrO_3 \quad (1)$$

On the other hand, in the sample 25A–75C_7A_3Z calcium monoaluminate ($CaAl_2O_4$) reacted simultaneously with Al_2O_3 to form unstable calcium dialuminate ($CaAl_4O_7$) under the same sintering condition. After sintering at 1400 °C, $CaAl_4O_7$ disappeared, the amount $Ca_7ZrAl_6O_{18}$ decreased and the amount of $CaAl_2O_4$ and $CaZrO_3$ increased. A quantitative approach based on XRD results in proposed mechanism of the chemical reaction 2:

$$Ca_7ZrAl_6O_{18} + CaAl_4O_7 + 2Al_2O_3 \rightarrow 7CaAl_2O_4 + CaZrO_3 \quad (2)$$

Following sintering at 1500 °C for 1 and 3 h, it was found that $Ca_7ZrAl_6O_{18}$ completely disappeared due to high-temperature eutectic reactions and formation of $Ca_{12}Al_{14}O_{33}$. The phase formation at each stage of sintering arising when several different reactions occur at different sintering condition will be discussed in detail later when discussing the microstructure evolution.

In 50A–50C_7A_3Z composite, a larger content of Al_2O_3 was enough to remain $CaAl_4O_7$ as a stable phase. At the temperature range between 1300 and 1500 °C the increment in $CaAl_4O_7$ content and the decrease in amount of both Al_2O_3 and initially formed $CaAl_2O_4$ phase were observed. Thus, the following reaction is proposed:

$$CaAl_2O_4 + Al_2O_3 \rightarrow CaAl_4O_7 \quad (3)$$

It was also found that evolution with temperature of the amount of crystalline phases present in the 75A–25C7A_3Z material occurred. So, Fig. 1c shows a remarkably strong increase with $CaAl_{12}O_{19}$ content and the accompanying decrease in content of both $CaAl_4O_7$ and Al_2O_3. The results of quantitative analysis of diffraction data support the proposed mechanism of reaction 4. In the alumina-rich part of the phase diagram calcium zirconate ($CaZrO_3$) not exists in equilibrium and then it must be converted in zirconia according to the chemical reaction 5.

$$CaAl_4O_7 + 4Al_2O_3 \rightarrow CaAl_{12}O_{19} \quad (4)$$

$$CaZrO_3 + Al_2O_3 \rightarrow CaAl_2O_4 + ZrO_2 \quad (5)$$

The final composition of investigated samples is presented as X-ray diffractograms in Figs. 2–4 with JCPDS standard cards used for phase identification.

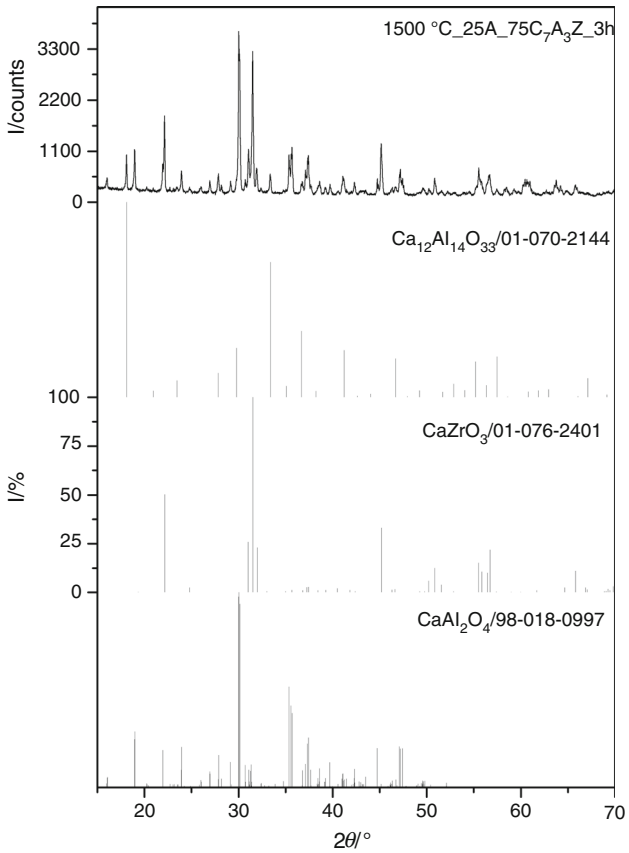

Fig. 2 X-ray diffraction pattern of the 25Al_2O_3–75C_7A_3Z composite sintered at 1500 °C for 3 h

Spectroscopic results

Figure 5 shows the IR spectrum of sintering products of Al_2O_3 and $Ca_7ZrAl_6O_{18}$ powders. FT-IR is suitable for analyzing the calcium aluminate phases and final characterization of CaO–Al_2O_3–ZrO_2 materials. According to paper presented by Tarte [21] concerning the infrared spectra of inorganic aluminates and characteristic vibrational frequencies of AlO_4 tetrahedra and AlO_6 octahedra, two different regions can be identified within the infrared spectra of calcium aluminates: the first one in the region of 700–900 cm^{-1} that corresponds to the stretching vibrations of a lattice of interlinked AlO_4 tetrahedra; and the second one appears in the region of 400–500 cm^{-1}, which can be particularly useful for determining the presence of bending mode of the AlO_4 lattice [22, 23]. In the spectrum of the main phase present in considered ceramic composite, $CaAl_2O_4$, the relevant signals are centered at 417, 447, 542, 573, 638, 687, 721, 764, 779, 790, 804, 820, 841 and

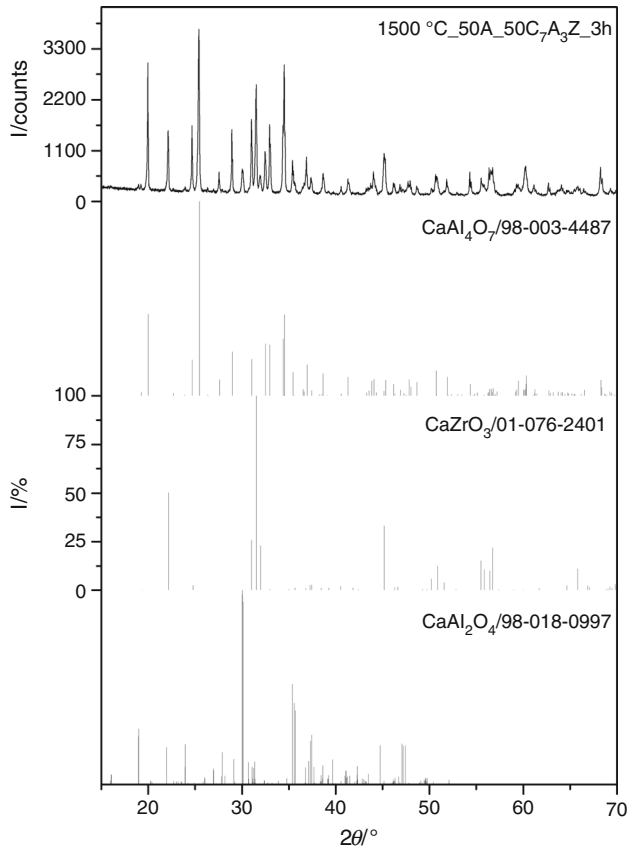

Fig. 3 X-ray diffraction pattern of the $50Al_2O_3$–$50C_7A_3Z$ composite sintered at 1500 °C for 3 h

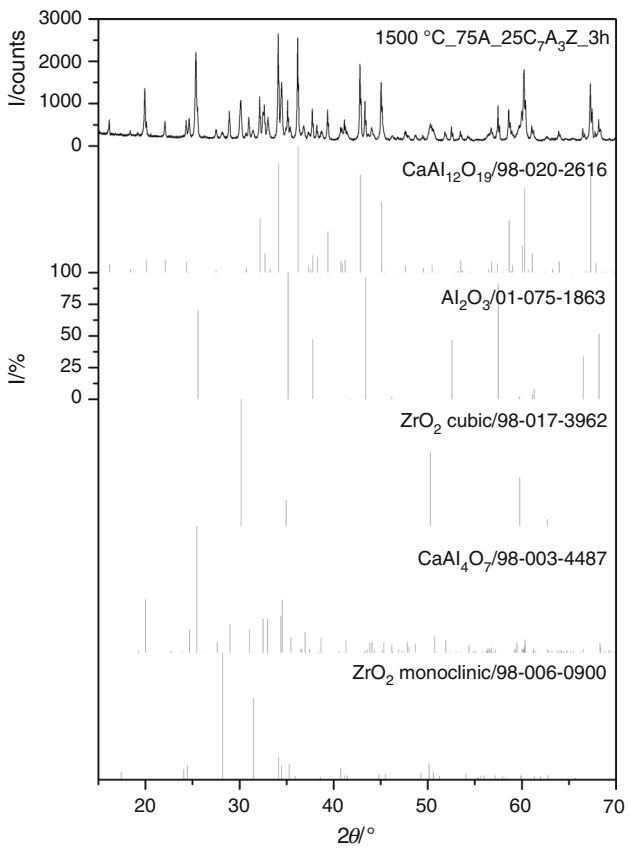

Fig. 4 X-ray diffraction pattern of the $75Al_2O_3$–$25C_7A_3Z$ composite sintered at 1500 °C for 3 h

868 cm^{-1}. The structural arrangement considered as the mentioned groups was also found in a minor phase of the $25Al_2O_3$–$75C_7A_3Z$ sample, i.e., $Ca_{12}Al_{14}O_{33}$. Despite the fact that dodecacalcium hepta-aluminate gives the spectrum with a very strong and broad absorption band with a maximum at 835–850 cm^{-1} and the two strong bands at 573–580 cm^{-1} and at 457–465 cm^{-1} [23, 24], the coincidence of positions of some bands in the IR spectra of the two phases occurred. The 50A–$50C_7A_3Z$ sample gives a spectrum dominated by the absorption bands of calcium dialuminate $CaAl_4O_7$ positioned at about 420, 442, 538, 573, 810, 834, 864, 918 and 943 cm^{-1}. The results are in very good agreement with the data presented in Ref. [22, 23]. These bands appear to coincide with some bands seen in the infrared spectrum of $CaAl_2O_4$. Similarly, IR-active fundamental band of calcium zirconate [25] is not clearly seen in this spectrum only showing up as a inflection point at 523 cm^{-1}.

The 75A–$25C_7A_3Z$ sample gives an extremely complicated spectrum (Fig. 5) due to the coincidence of positions of some bands in the IR spectra of $CaAl_{12}O_{19}$, α-Al_2O_3 and $CaAl_4O_7$. Thus, the appearance of intense absorption bands at 606 and 638 cm^{-1} may serve to identify the corundum

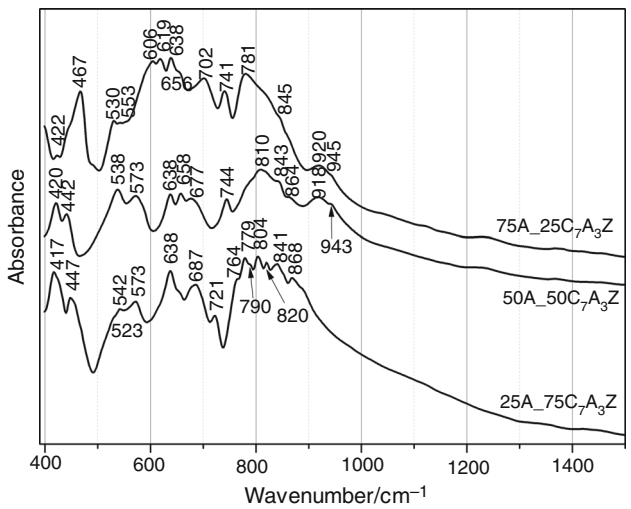

Fig. 5 FT-IR spectra of the $25Al_2O_3$–$75C_7A_3Z$, $50Al_2O_3$–$50C_7A_3Z$ and $75Al_2O_3$–$25C_7A_3Z$ composites obtained via sintering at 1500 °C for 3 h

being the representative compound, since its structure is built up by AlO_6 octahedra only [21]. In contrast, structure of calcium hexa-aluminate is based upon the structural arrangements where Al is distributed over three

symmetrically independent octahedral sites, one tetrahedral site, and one trigonal bipyramidal site [26]. Thus, by following the approach given in the paper [21] that the characteristic frequency ranges are as follow: "condensed" AlO_4 tetrahedra 700–900 cm^{-1}, "isolated" AlO_4 tetrahedra 650–800 cm^{-1}, "condensed" AlO_6 octahedra, 500–680 cm^{-1} and "isolated" octahedra AlO_6 400–530 cm^{-1}, the specific feature of the IR spectrum of $CaAl_{12}O_{19}$ is the presence of IR bands at about 400, 467, 530, 553, 619, 656, 702, 741, 788 and 945 cm^{-1} marked in the 75A–25C spectrum (Fig. 5). The peak positions of these bands are in very good agreement with those presented in Ref. [26]. However, it is important that some peak positions of $CaAl_{12}O_{19}$ coincide with the peak positions observed for the $CaAl_4O_7$. Characteristic IR absorption frequencies of $CaAl_4O_7$ were found within a very broad absorption peak located in the region between about 800 and 900 cm^{-1}. IR spectrum recorded for the prepared 75A–25C_7A_3Z sample is dominated by characteristic infrared absorption bands of functional groups belonging to some calcium aluminates, and it shows no significant band distinctive of cubic, tetragonal and monoclinic polymorphs of zirconia having their strong maxima at 480, 510 and 515 cm^{-1}, respectively [27].

Microstructural evolution

The mechanism of the high-temperature reactions between $Ca_7ZrAl_6O_{18}$ and Al_2O_3 was investigated based on the microstructure observations and chemical analysis with SEM–EDS. The BSE images of the polished cross sections of 25A–75C_7A_3Z and 75A–25C_7A_3Z composites sintered at 1300, 1400 and 1500 °C are shown in Figs. 6, 7. From these figures, it can be seen that during the first reaction stage at 1300 °C an attack of the alumina ions along the grain boundaries of calcium zirconium aluminate ($Ca_7ZrAl_6O_{18}$) occurred and calcium monoaluminate ($CaAl_2O_4$) and calcium zirconate ($CaZrO_3$) (Figs. 6 and 7, point 2) were then formed. This process proceeds according to the general balanced chemical reaction 1. Generally, high-temperature calcium zirconium aluminate ($Ca_7ZrAl_6O_{18}$) decomposition in the presence of Al_2O_3 and the further phase transformations can be explained by the phase diagram of the ternary system CaO–Al_2O_3–ZrO_2 [7, 9]. Let us consider the line joining the points represented by the composition of $Ca_7ZrAl_6O_{18}$ (CaO 47.8 mass%, Al_2O_3 37.2 mass%, ZrO_2 15.0 mass%) and Al_2O_3 100 mass%. Thus, when coarse-grained $Ca_7ZrAl_6O_{18}$ is combined and sintered with Al_2O_3 micropowder, the original $Ca_7ZrAl_6O_{18}$ grains will be rimmed by a reaction zone. The composition of this reaction zone could be expected by any point of the line $Ca_7ZrAl_6O_{18}$–Al_2O_3 within the ternary system CaO–Al_2O_3–ZrO_2. This means that the starting

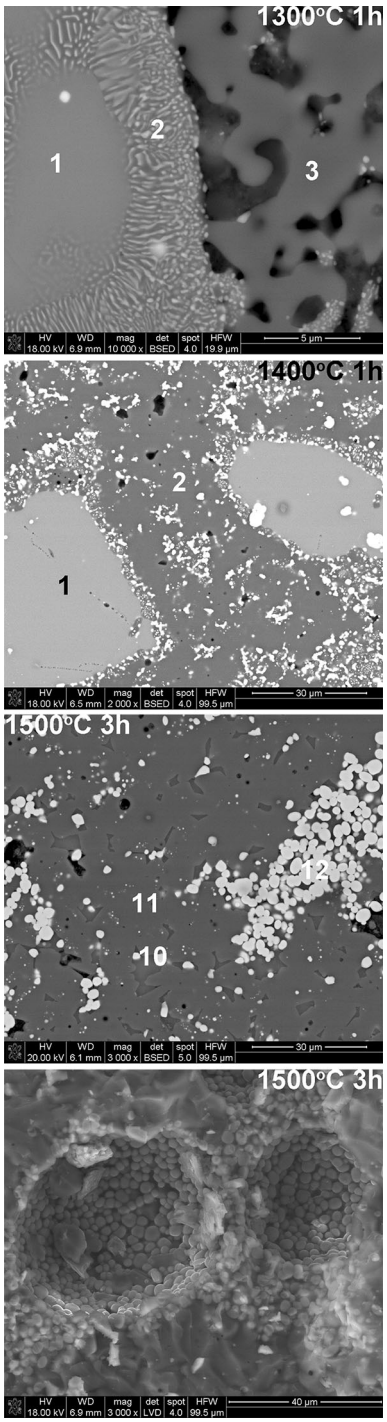

Fig. 6 SEM micrographs of the studied 25A–75C_7A_3Z composite sintered at 1300 °C (1 h), 1400 °C (1 h) and 1500 °C for 3 h (polished cross sections and fractured cross section). EDS analysis in spots: *1*—$Ca_7ZrAl_6O_{18}$, *2*—$CaZrO_3$ embedded in $CaAl_2O_4$ matrix, *3*—Al-rich $CaAl_2O_4$, *10*—$Ca_{12}Al_{14}O_{33}$, *11*—$CaAl_2O_4$ and *12*—coarse-grained $CaZrO_3$

powders will go through a series of chemical reactions before the final stable compounds are formed, with the intermediate compounds being non-equilibrium liquid or

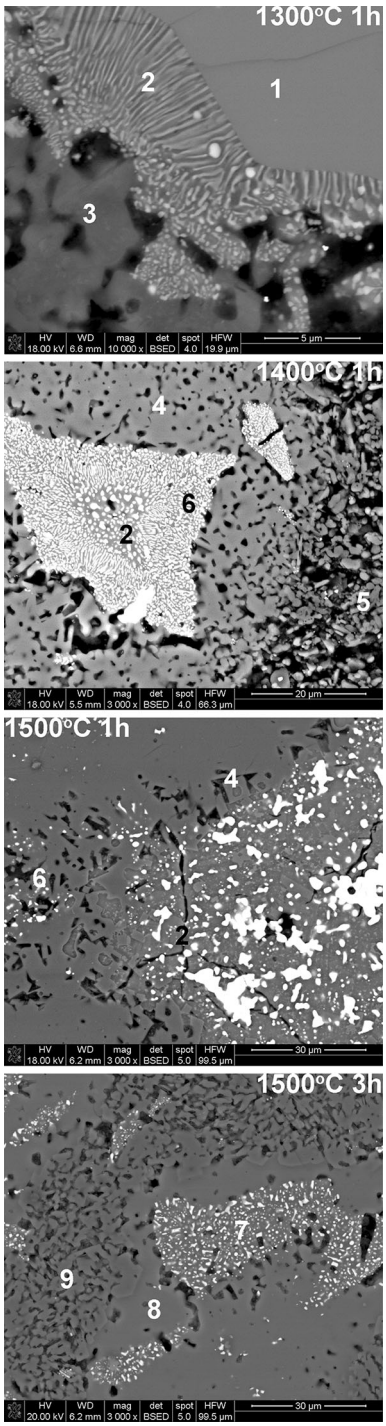

Fig. 7 SEM micrographs of the studied 75A–25C_7A_3Z composite sintered at 1300 °C (1 h), 1400 °C (1 h) and 1500 °C (1 and 3 h). EDS analysis in spots: *1*—$Ca_7ZrAl_6O_{18}$, *2*—$CaZrO_3$ embedded in $CaAl_2O_4$ matrix, *3*—Al-rich $CaAl_2O_4$, *4*—$CaAl_4O_7$, *5*—Al_2O_3, *6*—$CaZrO_3$ (coarse-grained) or ZrO_2 (fine-grained) embedded in $CaAl_4O_7$, *7*—ZrO_2 embedded in $CaAl_4O_7$ matrix, *8*—$CaAl_4O_7$ and *9*—$CaAl_{12}O_{19}$

solid transient phases. This process would start with reaction 1 and proceed according to the general balanced chemical reactions 3–5.

Due to the diffusion phenomena, the calcium zirconium aluminate grain was altered, having become mainly enriched in zircon and reduced in calcium. At the same time, Zr^{4+} ions may be considered rather as immobile during this process. Calcium zirconate, $CaZrO_3$, formed during reaction 1 tends to agglomerate in large oval grains embedded in calcium aluminate matrix ($xCaO{\cdot}yAl_2O_3$). Let us consider 25 mass% Al_2O_3–75 mass% $Ca_7ZrAl_6O_{18}$ sample where zirconium migration comes rather from the presence of liquid transient phase that produced the fully reacted ceramic composite. Another is to use starting powders wherein the proportion of ingredients in the starting dry mixture is as follows: 75 mass% Al_2O_3 and 25 mass% $Ca_7ZrAl_6O_{18}$ that will pass through a solid stage, rather than liquid, before the final microstructure is reached (Fig. 7, 1500 °C 3 h). Simultaneously, aluminum ions Al^{3+} move against a concentration gradient to increase their concentration inside $Ca_7ZrAl_6O_{18}$ grain core. As a result of an intense counter-diffusion of calcium ions and aluminum ions through reaction zone, the chemical equilibrium could be reached. Nevertheless, the final composition of the three phases in equilibrium, i.e., $Ca_7ZrAl_6O_{18}$–$CaZrO_3$–$CaAl_2O_4$ and $CaAl_4O_7$–ZrO_2–$CaAl_{12}O_{19}$ was not received as it was expected for both 25A–75C_7A_3Z and 75A–25C_7A_3Z, respectively. The investigation of the microstructural evolution within the 75A–25C_7A_3Z sample confirmed by XRD and FT-IR analysis has shown that the thermodynamic equilibrium was not reached due to the presence of both Al_2O_3 and $CaAl_4O_7$ non-equilibrium phases that could undergo of transition according to reaction 4. Hence, final microstructure of the 75A–25C_7A_3Z ceramics achieved at 1500 °C and 3 h sintering consist of ZrO_2 particles embedded in the $CaAl_4O_7$ phase (Fig. 7, point 7) occurring in the initial region of $Ca_7ZrAl_6O_{18}$ grain and $CaAl_{12}O_{19}$ (Fig. 7, point 9). Additionally, the 75A–25C_7A_3Z composite cement consists of alumina as checked by XRD and FT-IR.

Calorimetric studies

The heat of hydration was measured for the grounded cementitious materials (reference compounds and composite cements) whose particle size distribution known as the median diameter or the medium value of the particle size distribution was about 30 μm. A reference measurement of hydration heat of single component, i.e., $CaAl_2O_4$ (CA), $CaAl_4O_7$ (CA_2), $Ca_{12}Al_{14}O_{33}$ ($C_{12}A_7$) and $Ca_7ZrAl_6O_{18}$ (C_7A_3Z) (Fig. 8) using isothermal heat flow calorimeter at 25 °C was a useful tool for both studying and assessing the hydration behavior of these cementitious compounds.

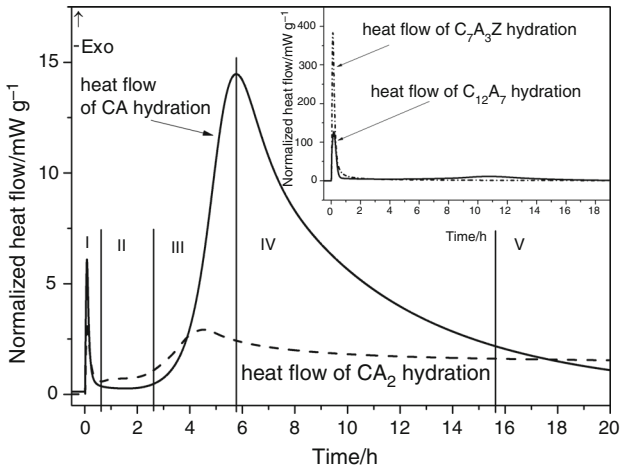

Fig. 8 Heat flow curves of reference materials, i.e., $CaAl_2O_4$-, $CaAl_4O_7$-, $Ca_7ZrAl_6O_{18}$-, $Ca_{12}Al_{14}O_{33}$-based cementitious pastes prepared with w/s = 1.0 hydrated at 25 °C. Heat flow curves normalized to mass of binder paste (with in situ mixing)

The heat flow curves for the 25A_75C_7A_3Z, 50A_50C_7A_3Z and 75A_25C_7A_3Z hydrating multiphase cement pastes prepared with a water/solid ratio of 1.0 at 25 °C are shown in Fig. 9a–c, respectively. Looking at the overall results, some relationships have been noticed in observations. Firstly, the heat flow peaks of all composite cements are strongly enhanced by the presence of Ca-containing phases (Fig. 9a–c). It means an increase in the peak intensity of heat flow of hydration with decreasing the $Al_2O_3/Ca_7ZrAl_6O_{18}$ mass ratio of the starting mixtures, as shown in Fig. 9a–c. Interestingly, intensity of the heat flow peak of composite cements belonging to the system CaO–Al_2O_3–ZrO_2 hydration is also strongly reduced with the degree of conversion of $Ca_7ZrAl_6O_{18}$ within the temperature range from 1300 to 1500 °C. As may be also seen, the hydration of all multiphase composite cements is accelerated with increasing the $Al_2O_3/Ca_7ZrAl_6O_{18}$ mass ratio of the starting mixtures. The induction period was shortened, and the second exothermic heat effect was accelerated considerably as the Al_2O_3 amount increased. The influence of alumina on the hydration of Ca-aluminates is a phenomenon well known [28].

Going into details, presented figures (Fig. 9a–c) illustrate the hydraulic activity of each cements, especially, the hydration kinetics of individual constituent phases and the mutual interaction of these constituents. Test results indicated that the phase composition of particular cements expressed in mass percent (Fig. 1a–c) of the possible constituent hydraulic phases, i.e., $CaAl_2O_4$ (CA), $CaAl_4O_7$ (CA_2), $Ca_7ZrAl_6O_{18}$ (C_7A_3Z) and $Ca_{12}Al_{14}O_{33}$ ($C_{12}A_7$) and/or Al_2O_3 (A) strongly affects the microcalorimetric curve obtained in the isothermal conditions. Thus, these curves reflect the rate of heat

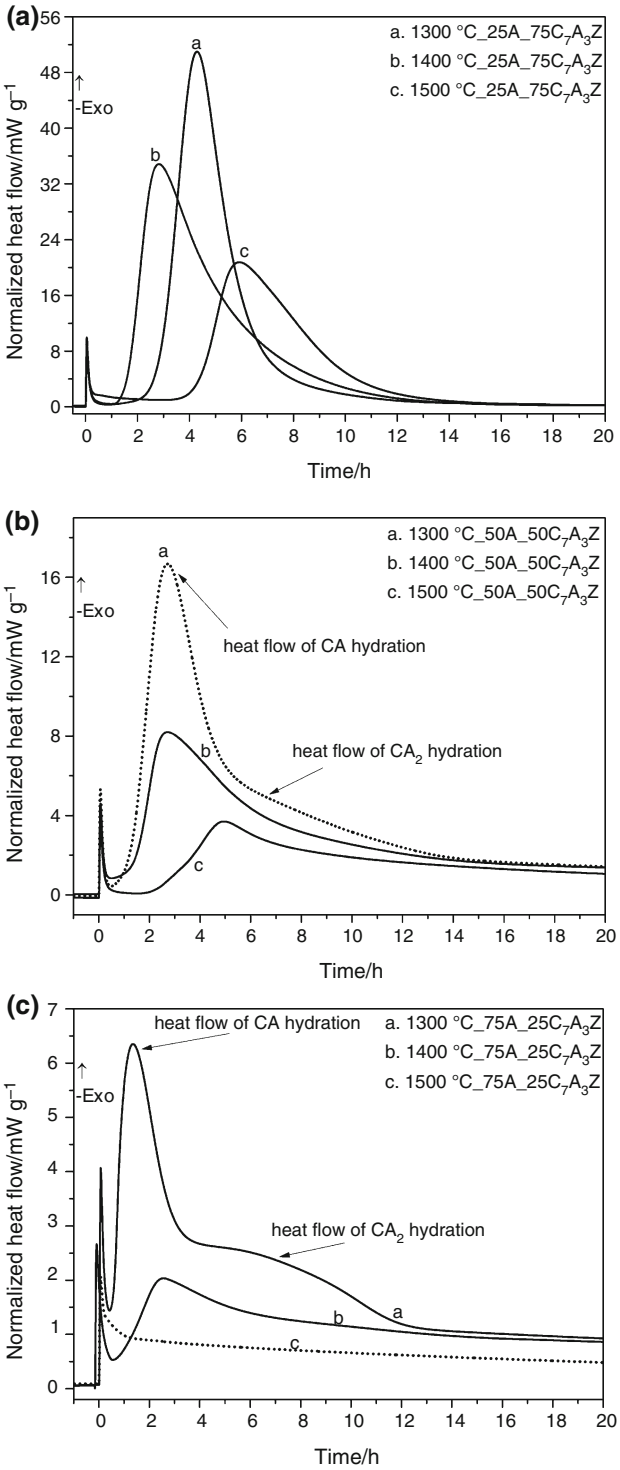

Fig. 9 Heat flow curves of 25A_75C_7A_3Z (**a**), 50A_50C_7A_3Z (**b**) and 75A_25C_7A_3Z (**c**) pastes hydrated at 25 °C for w/s = 1.0, normalized to mass of binder paste (with in situ mixing). Cements obtained at 1300, 1400 and 1500 °C

evolution vs. time for each considered composite cements from the system CaO–Al_2O_3–ZrO_2. It is well known that some stages of reaction can be identified on the

calorimetric curve, namely: the pre-induction (the heat of wetting effect), induction (II), hydration rate increase (III), hydration rate decrease (IV) and low hydration rate (V), respectively. Thus, calcium monoaluminate hydration (Fig. 8) can be considered as good model of cement reaction with water. It is clearly visible that the shape of the heat flow curves of hydrating cement pastes is characteristic and the observed differences relate mainly to the stages generically, but each one can have different duration depending on the cement mineral composition. The all calorimetric curves shown in Fig. 9a–c exhibit one major feature, an intense first heat peak which occurs immediately after injection and mixing the water with the dry cement powders. This quick release of heat is associated with the wetting and initial dissolution of the cement particles within a few minutes after adding water. Besides, the rate evolution during hydration of the samples heat treated at 1300 °C (samples 75A_25C_7A_3Z, 50A_50C_7A_3Z, 25A_75C_7A_3Z) and 1400 °C (sample 25A_75C_7A_3Z) for this peak is strongly enhanced by the presence of the highly reactive calcium zirconium aluminate ($Ca_7ZrAl_6O_{18}$) phase (Figs. 1a–c). The highly reactive nature of $Ca_7ZrAl_6O_{18}$ has been extensively studied in recent years [9, 11].

Microcalorimetric curves of the 25A_75C_7A_3Z samples (Fig. 9a-a–c) are strongly dominated by the intense exothermic heat associated with CA ($CaAl_2O_4$) hydration. It is shown that C_7A_3Z (1300 °C_25A_75C_7A_3Z, 1400 °C_25A_75C_7A_3Z) exhibits a strong accelerating effect, more effective than $C_{12}A_7$ (1500 °C_25A_75C_7A_3Z), on the hydration of calcium monoaluminate (CA).

The hydration of 50A_50C_7A_3Z composite cements is characterized by a heat flow peak with dissimilar acceleration rate and intensity which follows the induction period. The hydration of 1300 °C_50A_50C_7A_3Z cement is characterized by a double heat flow peak with different rate and intensity. Thus, the different behaviors, as regards hydration kinetics, of CA and CA_2 are indicated. The hydration reactions of calcium monoaluminate (CA) precede the reaction of CA_2 with water which, on the other hand, has the ability to very slow and lengthy reaction. The length of the induction period of 50A_50C_7A_3Z samples hydration has been found to be related to both CA and CA_2 contents and increased with increasing CA_2 content within the temperature range from 1300 to 1500 °C. Therefore, it is appropriate to say that CA phase acts as an accelerating agent for the hydration of CA_2 phase.

Microcalorimetric curve of the 1500 °C_75A_25C_7A_3Z sample (Fig. 9c-c.) is strongly dominated by the first stage, i.e., the initial wetting of the cement particles and by the second not intense exothermic heat (a weak diffuse exothermic effect) associated with CA_2 ($CaAl_4O_7$) hydration. Analyzing the graphs of the composite cements heat treated for 1 h at 1300 and 1400 °C, I observe the well-known accelerating effect of other aluminate compound on the hydration of CA_2. Increase in the reactivity of CA_2 was accomplished by the presence of reactive phases combinations like CA/C_7A_3Z (Fig. 9c-a) and CA (Fig. 9c-b). Interestingly, the hydraulic behavior of both CA_2 and CA is strongly enhanced by the presence of C_7A_3Z.

Discussion

In this paper, a new approach for synthesizing composite-designed CaO–Al_2O_3–ZrO_2 cements via the high-temperature reactions within the $Ca_7ZrAl_6O_{18}$–Al_2O_3 system in the temperature range between 1300 and 1500 °C was proposed. The reaction products formed in these samples were well understood by looking at compatibility triangles across the line joining Al_2O_3 and $Ca_7ZrAl_6O_{18}$ of the CaO–Al_2O_3–ZrO_2 phase diagram [7]. The configurations of three-phase regions in equilibrium are the following: I. $Ca_7ZrAl_6O_{18}$–$CaAl_2O_4$–$CaZrO_3$, II. $CaAl_2O_4$–$CaZrO_3$–$CaAl_4O_7$, III. $CaAl_4O_7$–$CaZrO_3$–ZrO_2, IV. $CaAl_4O_7$–ZrO_2–$CaAl_{12}O_{19}$ and V. $CaAl_{12}O_{19}$–ZrO_2–Al_2O_3. The phase transformation in the prepared samples 25 mass% Al_2O_3–75 mass% $Ca_7ZrAl_6O_{18}$, 50 mass% Al_2O_3–50 mass% $Ca_7ZrAl_6O_{18}$ and 75 mass% Al_2O_3–25 mass% $Ca_7ZrAl_6O_{18}$ having the initial phase composition in I, II and IV triangles, respectively, sintered in the temperature range 1300–1500 °C was investigated with X-ray diffraction (XRD), Rietveld XRD Quantification, infrared spectroscopy (IR) and scanning electron microscopy combined with energy-dispersive spectrometry (SEM/EDS) techniques. Final results from the various analytical techniques revealed that phase composition of the calcia–zirconia–alumina composite cements prepared via the high-temperature reactions between $Ca_7ZrAl_6O_{18}$ and Al_2O_3 differs from the strategically designed sample composition due to sintering at different experimental conditions. It was concluded that the 75 mass% Al_2O_3–25 mass% $Ca_7ZrAl_6O_{18}$ specimen was probably not fully equilibrated at 1500 °C due to the predominant diffusion path in solid-state reactions. The 25 mass% Al_2O_3–75 mass% $Ca_7ZrAl_6O_{18}$ and 50 mass% Al_2O_3–50 mass% $Ca_7ZrAl_6O_{18}$ specimens were fully equilibrated at temperatures of 1400 and 1500 °C, respectively.

Calcium zirconium aluminate ($Ca_7ZrAl_6O_{18}$) was unstable when it was heated with alumina, and it was subjected to chemical reactions with the formation of calcium aluminates increasingly richer in aluminum oxide ($Ca_7ZrAl_6O_{18}$ → $CaAl_2O_4$ → $CaAl_4O_7$ → $CaAl_{12}O_{19}$) and Zr-bearing compounds ($CaZrO_3$ or ZrO_2). Investigations by SEM showed that calcium zirconate tends to be uniformly distributed and as rounded oval grains within the calcium aluminate matrix

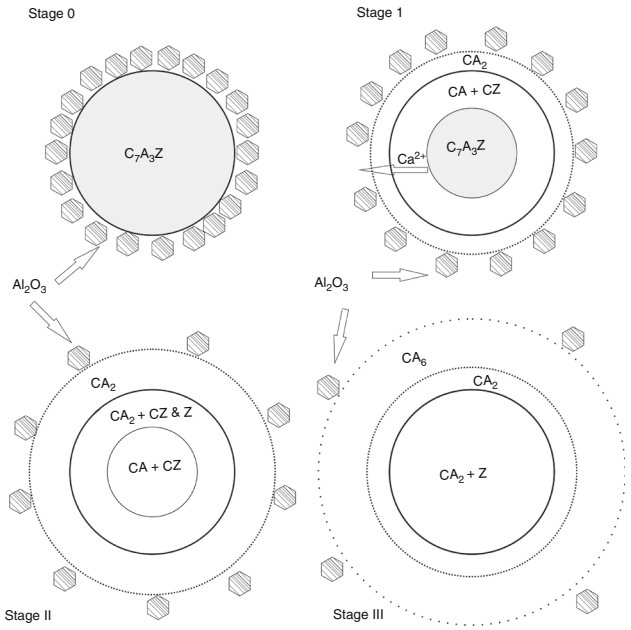

Fig. 10 Schematic diagram of phase distribution sequence in the reaction zone of the binary mixture like $Ca_7ZrAl_6O_{18}$–Al_2O_3

with a high CaO/Al_2O_3 molar ratio corresponding to $C_{12}A_7$ ($C \equiv CaO$, $A \equiv Al_2O_3$) in the final microstructure. On the other hand, fine-grained zirconia were concentrated in microareas of the initial $Ca_7ZrAl_6O_{18}$ grains, and it was embedded in the Al-richer calcium aluminate matrix. Based on theoretical considerations on the reaction mechanism in the CaO–Al_2O_3–ZrO_2 system and the presented results it may be supposed that the reactions at the single-grain level would proceed from the stage 0 to III, which is graphically presented in Fig. 10.

The hydration process of composite cements belonging to the system CaO–Al_2O_3–ZrO_2 was characterized by the different intensity exothermic reactions. The shape of the heat flow curves resulted from calorimetric measurements reflects the cement hydration process. The proportion of the selected $CaAl_2O_4$, $CaAl_4O_7$, $Ca_{12}Al_{14}O_{33}$, $Ca_7ZrAl_6O_{18}$ or Al_2O_3 phases changes the shape of the heat flow curve, so the hydraulic reactivity of cement phases and their mutual influence on hydration behavior can be quantified.

Conclusions

Some general conclusions can be drawn based on the results of this work:

1. Reactive sintering process of $Ca_7ZrAl_6O_{18}$ and Al_2O_3 micropowders is an effective way for production of novel composite cements belonging to the system CaO–Al_2O_3–ZrO_2.
2. The designed compositions of these hydraulic binders can be achieved with factors such as: ratio by mass of $Ca_7ZrAl_6O_{18}$ to Al_2O_3, time and sintering temperature.
3. The shrinking core model in which the particle size of $Ca_7ZrAl_6O_{18}$ is being consumed by reaction with alumina can be applied to visualization of reactions involving changes in microareas of unreacted core.
4. Phase composition affects the hydration kinetics of hydraulic binders determined using isothermal calorimetry.
5. Due to this unique combination of properties, novel composite cements belonging to the system CaO–Al_2O_3–ZrO_2 can be used in many types of unshaped refractory materials including castables.

Acknowledgements The research was performed at Faculty of Materials Science and Ceramics of AGH and was partly supported by the Project No. 11.11.160.617.

References

1. Zaitsev AI, Korolyov NV, Mogutnov BM. Phase equilibria in the CaF_2–Al_2O_3–CaO system. J Mater Sci. 1991;26(6):1588–600.
2. Zaitsev AI, Litvina AD, Mogutnov BM. Thermochemistry of oxide-fluoride flux systems. High Temp Sci. 1990;28:351–77.
3. Iftekhar S, Grins J, Svensson G, Lööf J, Jarmar T, Botton GA, Andrei CM, Engqvist H. Phase formation of $CaAl_2O_4$ from $CaCO_3$–Al_2O_3 powder mixtures. J Eur Ceram Soc. 2008;28:747–56.
4. Jonas S, Nadachowski F, Szwagierczak D. A new non-silicate refractory of low thermal expansion. Ceram Int. 1998;24:211–6.
5. Jonas S, Nadachowski F, Szwagierczak D. Low thermal expansion refractory composites based on $CaAl_4O_7$. Ceram Int. 1999;25:77–84.
6. Jonas S, Nadachowski F, Szwagierczak D, Wójcik G. Thermal expansion of $CaAl_4O_7$-based refractory compositions containing MgO and CaO additions. J Eur Ceram Soc. 2006;26:2273–8.
7. Berezhnoi AS, Kordyuk RA. Melting diagram of the system CaO–Al_2O_3–ZrO_2. Dopov Akad Nauk URSR. 1963;10:1344–7.
8. Fukuda K, Iwata T, Nishiyuki K. Crystal structure, structural disorder, and hydration behavior of calcium zirconium aluminate, $Ca_7ZrAl_6O_{18}$. Chem Mater. 2007;19(15):3726–31.
9. Madej D, Szczerba J, Nocuń-Wczelik W, Gajerski R. Hydration of $Ca_7ZrAl_6O_{18}$ phase. Ceram Int. 2012;38(5):3821–7.
10. Madej D, Szczerba J, Nocuń-Wczelik W, Gajerski R, Hodur K. Studies on thermal dehydration of the hydrated $Ca_7ZrAl_6O_{18}$ at different water–solid ratios cured at 60°C. Thermochim Acta. 2013;569:55–60.
11. Madej D, Szczerba J. Study of the hydration of calcium zirconium aluminate ($Ca_7ZrAl_6O_{18}$) blended with reactive alumina by calorimetry, thermogravimetry and other methods. J Therm Anal Calorim. 2015;121:579–88.
12. Lee J-H, Mori T, Li J-G, Ikegami T, Takenouchi S. The influence of alumina addition and its distribution upon grain-boundary conduction in 15 mol.% calcia-stabilized zirconia. Ceram Int. 2001;27:269–76.
13. Liu R, Li Y, Wang C-A, Tie S. Fabrication of porous alumina-zirconia ceramics by gel-casting and infiltration methods. Mater Design. 2014;63:1–5.

14. Ai Y, Xie X, He W, Liang B, Fan Y. Microstructure and properties of $Al_2O_{3(n)}/ZrO_2$ dental ceramics prepared by two-step microwave sintering. Mater Design. 2015;65:1021–7.
15. Tian Y, Pan X, Yu H, Tu G. Formation mechanism of calcium aluminate compounds based on high-temperature solid-state reaction. J Alloys Compd. 2016;670:96–104.
16. Bruni YL, Garrido LB, Aglietti EF. Properties of $CaO–ZrO_2$ based composites. Procedia Mater Sci. 2015;8:203–10.
17. Sktani ZDI, Azhar AZA, Ratnam MM, Ahmad ZA. The influence of in situ formation of hibonite on the properties of zirconia toughened alumina (ZTA) composites. Ceram Int. 2014;40:6211–7.
18. Pięta A, Bućko MM, Januś M, Lis J, Jonas S. Calcium hexaaluminate synthesis and its influence on the properties of $CA_2–Al_2O_3$-based refractories. Ceram Int. 2015;35(16):4567–71.
19. PFR 20 Product Brochure, Alteo Company.
20. ICDD and ICSD PDF-2 database products.
21. Tarte P. Infra-red spectra of inorganic aluminates and characteristic vibrational frequencies of AlO_4 tetrahedra and AlO_6 octahedra. Spectrochim Acta A Mol Spectrosc. 1967;23(7):2127–43.
22. Torréns-Martín D, Fernández-Carrasco L, Martínez-Ramírez S. Hydration of calcium aluminates and calcium sulfoaluminate studied by Raman spectroscopy. Cem Concr Res. 2013;47:43–50.
23. Fernández-Carrasco L, Torrens-Martín D, Morales LM, Martínez-Ramírez S. In: Theophanides T, editor. Infrared spectroscopy in the analysis of building and construction materials, infrared spectroscopy—materials science, engineering and technology. InTech. ISBN 978-953-51-0537-4. doi:10.5772/36186. http://www.intechopen.com/books/infrared-spectroscopy-materials-science-engineering-and-technology/infrared-spectroscopy-of-cementitious-materials.
24. Kokhman AG, Zhmoidin GI. Vibrational spectra of $12CaO·7Al_2O_3$ and $5CaO·3Al_2O_3$ crystals. J Appl Spectrosc. 1981;35(6):1322–6.
25. Orera VM, Pecharromán C, Peña JI, Merino RI, Serna CJ. Vibrational spectroscopy of $CaZrO_3$ single crystals. J Phys Condens Matter. 1998;10:7501–10.
26. Hofmeister AM, Wopenka B, Locock AJ. Spectroscopy and structure of hibonite, grossite, and $CaAl_2O_4$: implications for astronomical environments. Geochim Cosmochim Acta. 2004;68(21):4485–503.
27. Phillippi CM, Mazdiyasni KS. Infrared and Raman spectra of zirconia polymorphs. J Am Ceram Soc. 1971;54(5):254–8.
28. Rettel A, Seydel R, Gessner W, Bayoux JP, Campas A. Investigations on the influence of alumina on the hydration of monocalcium aluminate at different temperatures. Cem Concr Res. 1993;23:1056–64.